# Effect of intrinsic curvature on semiflexible polymers

Surya K. Ghosh, Kulveer Singh, and Anirban Sain*
*Physics Department, Indian Institute of Technology-Bombay, Powai, Mumbai 400076, India*
(Received 21 April 2009; published 5 November 2009)

Recently many important biopolymers have been found to possess intrinsic curvature. Tubulin protofilaments in animal cells, FtsZ filaments in bacteria and double stranded DNA are examples. We examine how intrinsic curvature influences the conformational statistics of such polymers. We give exact results for the tangent-tangent spatial correlation function $C(r)=\langle \hat{t}(s).\hat{t}(s+r)\rangle$, both in two and three dimensions. Contrary to expectation, $C(r)$ does not show any oscillatory behavior, rather decays exponentially and the effective persistence length has strong length dependence for short polymers. We also compute the distribution function $P(\mathbf{R})$ of the end to end distance $\mathbf{R}$ and show how curved chains can be distinguished from wormlike chains using loop formation probability.

DOI: 10.1103/PhysRevE.80.051904 PACS number(s): 87.15.H−, 87.16.Ka, 36.20.Ey, 82.35.Pq

A cell hosts variety of polymeric filaments. Tubulin filaments in eukaryotic organisms and FtsZ filaments in prokaryotic organisms, are important members of the cellular cytoskeleton. They also play important role during cell division. Therefore *in vitro* properties of these filaments, both in their isolated filament form as well as in bundled form, have been of great interest [1–3]. One of the important mechanical properties which tubulin and FtsZ filaments share is their intrinsic curvature. The mechanisms by which microtubules generate pulling force during chromosome segregation [1] and FtsZ-ring generates contractile radial force during cell constriction [4], exploit their intrinsic curvature.

Interestingly biopolymers with intrinsic curvature and torsion have been known for long. Prominent examples are the alpha helices in proteins. They have also been extensively modeled [5]. But polymers with only intrinsic curvature (but no intrinsic torsion), have not received much attention. This is perhaps because the helical structures are visually easy to detect compared to intrinsic curvature without torsion, except in two dimensions (2D). Intrinsic curvature is evident in electron microscope [2] and atomic force microscope (AFM) [3] pictures of FtsZ and AFM pictures DNA [6]. As our analysis will reveal, in three dimensions (3D), unless both $L/l_p$ and $l_p/R_0$ are of order one, where $R_0$ is the intrinsic radius of curvature of the polymer, $L$ its contour length and $l_p$ its persistence length, it is difficult to differentiate them, visually, from a WLC. In this paper we will focus on conformational properties of curved chains, that may distinguish it from a WLC. Such diagnostic markers are important in the context of ever increasing number of new biopolymers, with properties which cannot be explained by the standard models such as flexible Gaussian chains or WLC [7], especially for short contour lengths. We ignore excluded volume effects and self crossings which are negligible if $L/R_0 \leq 1$; but important otherwise, as well as for nondilute polymer solutions. Interplay of the additional length scale $R_0$ with $l_p$ and $L$ is of interest here.

Equilibrium, conformational statistics of such curved polymers have been studied using Monte Carlo simulation [8] and auxiliary field theory [9]. Their dynamics have been studied by numerical solution of their nonlinear equation of motion [10]. The field theoretic calculation [9] assumed zero average torsion for the curved polymer and used a spatially varying auxiliary field. They predicted an oscillatory decay $C(r)\sim e^{-r/\tilde{l}_p}\cos(r/R_0)$ for the correlation function in three dimensions. Here $\tilde{l}_p$ is the effective persistence length. This oscillatory decay is geometrically suggestive, as the polymer may wind around itself (loop) due to its intrinsic curvature. This also implies that at large $l_p$, for $L>2\pi R_0$ the peak of the distribution function $P(\mathbf{R})$ of the end to end distance $R$ will alternate between $R=0$ and $R=2R_0$, corresponding to complete loops and half loops, respectively, as the length $L$ is increased.

We compute $C(r)$ exactly both in 2D and 3D and show that the decay is purely exponential, while oscillations can be recovered in 2D through extra constraint on the sign of the preferred interbond angle and through imposing torsion in 3D [5]. The absence of oscillations can be understood as follows. Although intrinsic curvature constrains the magnitude of the local curvature $|\frac{d\hat{t}(s)}{ds}|\sim R_0^{-1}$, the direction of the curvature vector $\frac{d\hat{t}(s)}{ds}$ remain uncorrelated along the contour, leading to exponential decorrelation. In other words the local plane of curvature keeps changing randomly which disfavors formation of planar or helical loops. Although the functional form of $C(r)$ cannot distinguish WLC from curved chains, the effective persistence length $\tilde{l}_p$ turns out to be $N$ dependent. We also compute the distribution function $P(\mathbf{R})$ for curved chains which shows difference with WLC.

A polymer of length $L$ is described by a space curve $\mathbf{R}(s), s\in[0,L]$. The Hamiltonian of an intrinsically curved polymer is given by [10], $\frac{H}{K_BT}=\frac{l_p}{2}\int_{s=0}^{L}[\kappa(s)-R_0^{-1}]^2ds$. The curvature vector $\vec{\kappa}(s)=\frac{d\hat{t}(s)}{ds}$, where $\hat{t}(s)$ is the local tangent to the curve $[\hat{t}(s)=\frac{d\mathbf{R}(s)}{ds}]$ and $R_0$ is the intrinsic radius of curvature. Changing variable $x=\frac{s}{l_p}$, $\frac{H}{K_BT}=\frac{1}{2}\int_{x=0}^{L/l_p}(|\frac{d\hat{t}(x)}{dx}|-\frac{l_p}{R_0})^2dx$. This reveals that $l_p/L$ and $l_p/R_0$ are the two important dimensionless ratios of the problem. In the discrete limit the monomers are given by the position vectors $\mathbf{R}_i$ and the normalized bond vectors are $\hat{t}_i=(\mathbf{R}_{i+1}-\mathbf{R}_i)/b$, where $b$ is the bond length. The discretized Hamiltonian reads

*asain@phy.iitb.ac.in

 

$$\frac{H}{k_BT} = \sum_{i=1}^{N-1} h_i = \frac{1}{2}\sum_{i=1}^{N-1}\left\{\frac{|\hat{t}_{i+1}-\hat{t}_i|}{\sqrt{\Delta}} - \frac{l_p\sqrt{\Delta}}{R_0}\right\}^2, \quad (1)$$

where $\Delta=\frac{L/l_p}{N}$. Since the Hamiltonian depends only on nearest neighbor bond angles, we can use a standard property [11], $\langle \hat{t}_i.\hat{t}_k\rangle=\langle \hat{t}_i.\hat{t}_{i+1}\rangle^{|k-i|}$. This yields $\langle \hat{t}(s).\hat{t}(s+r)\rangle = \exp(-r/\tilde{l}_p)$, where the spatial separation $r=b|k-i|$. Thus quite counterintutively, in 3D, $C(r)$ does not show any oscillation, but decays as $\exp(-r/\tilde{l}_p)$. We identify the effective persistence length as $\tilde{l}_p=-b/\ln\langle \hat{t}_i.\hat{t}_{i+1}\rangle$ and $\langle \hat{t}_i.\hat{t}_{i+1}\rangle=\frac{\int d\Omega_i \cos\theta_i e^{-h_i(\theta_i)}}{\int d\Omega_i e^{-h_i(\theta_i)}}$. Here $\theta_i$ is the angle between $\hat{t}_i$ and $\hat{t}_{i+1}$ and the integration is done by holding $\hat{t}_i$ as the polar axis and integrating $\hat{t}_{i+1}$ over the solid angle $\Omega_i$. The thermal weight is $\exp(-h_i)$, where $h_i(\theta_i)=[\frac{\sqrt{1-\cos\theta_i}}{\sqrt{\Delta}}-\frac{l_p\sqrt{\Delta}}{\sqrt{2}R_0}]^2$ [see Eq. (1)]. $\langle \hat{t}_i.\hat{t}_{i+1}\rangle$ is given by

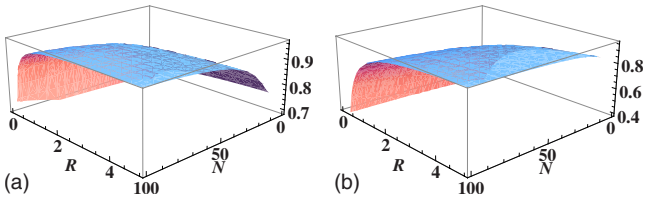


FIG. 1. (Color online) The effective persistence length $\tilde{l}_p/l_p$ with respect to $R_0$ and $N$, at $l_p/L=0.2$ (left) and $l_p/L=10$ (right).

$$e^{-y^2}[2\sqrt{N}R_0(-L^2l_p-2LNR_0^2+2l_pN^2R_0^2+\exp\left[\frac{2l_p}{R_0}\right]^{-y_1^2}[L^2l_p+2l_pN^2R_0^2+2LNR_0(l_p+R_0)])$$
$$-e^{y^2}\sqrt{2\pi Ll_p}(L^2l_p+3LNR_0^2-2l_pN^2R_0^2)\{erf[y]-erf[y-y_1]\}]/[2l_pN^2R_0^2(2\sqrt{N}R_0e^{-y^2-y_1^2}\{e^{y_1^2}-e^{\frac{2l_p}{R_0}}\}$$
$$+\sqrt{2\pi Ll_p}\{erf[y]-erf[y-y_1]\})], \quad (2)$$

where $y=\sqrt{Ll_p/2N}/R_0$, $y_1=\sqrt{2Nl_p/L}$. Using this expression we plot $\tilde{l}_p/l_p$ in Fig. 1 as a function of $R_0$ and $N$. At finite $R_0, L$, but large $N$, $\tilde{l}_p/l_p\to 1$. But interestingly the discreteness of the chain has practical importance. For example, DNA has a finite bond length approximately equal to the size of a base pair (bp) and experiments with short DNA strands (15–90 bp) have revealed [12] an apparent persistence length which is three to four times lesser than the standard value $\sim$50 nm (150 *bp*). To explain this Ref. [12] has ivoked new physics at the scale of base pairs. Models with long range correlation in the intrinsic curvature disorder in base pairs has also been proposed [6]. But our calculation shows that a simpler factor, such as an uniform curvature can lead to substantial decrease in $\tilde{l}_p$. Figure 1 shows that for low $R_0$ and high $l_p$ the reduction in $\tilde{l}_p$ could be twofolds.

Since most curved polymers have been detected on 2D substrates, 2D requires special attention. We will now compute $C(r)$ in 2D. Here the angle between the bond vectors $\hat{t}_i$ and $\hat{t}_k$, $\theta_{i,k}$ can be written as a sum of the intermediate angles between the successive bond vectors. Denoting $k=i+l$, $\theta_{i,i+l}=\Sigma_{j=i}^{k-1}\theta_{j,j+1}$. Note that the sign of the angles are important here and $\theta_{j,j+1}$ is defined as the angle the $\hat{t}_{j+1}$ vector has to rotate with respect to the $\hat{t}_j$ vector, and thus $C(r)$ is given by

$$\langle \cos\theta_{i,i+l}\rangle = \mathrm{Re}\langle e^{i\Sigma_{j=i}^{k-1}\theta_{j,j+1}}\rangle = \mathrm{Re}\left[\frac{\int d\theta e^{i\theta}e^{-h(\theta)}}{\int d\theta e^{-h(\theta)}}\right]^l. \quad (3)$$

Note that if the symmetry of $h(\theta)$ with respect to $\pm\theta$ is not broken then the integrals $\int_{-\pi}^{\pi}$ are real and hence $\langle \cos\theta_{i,i+l}\rangle$ will decay exponentially, as in 3D. The integral can be estimated by noting that the numerator gets its maximum contribution from $\theta=\theta_0$ (and not $-\theta_0$, to break the symmetry) where the exponent $[\frac{\sqrt{1-\cos\theta_0}}{\sqrt{\Delta}}-\frac{l_p\sqrt{\Delta}}{\sqrt{2}R_0}]$ is zero. In the continuum limit $(b/R_o\ll 1)$ the maximum occurs at a small value of $\theta_0\simeq b/R_0$ which allows the approximation $\cos\theta\simeq 1-\frac{\theta^2}{2}$. The resulting integral can be evaluated analytically [Eq. (4)] and its agreement with the numerical evaluation of the exact integral in Eq. (3) is excellent (figure not shown).

$$\mathrm{Re}\left\{\left[\frac{\int_{-\pi}^{\pi}e^{i\theta}e^{-\frac{y_1^2}{2}(\theta-\theta_0)^2}d\theta}{\int_{-\pi}^{\pi}e^{-\frac{y_1^2}{2}(\theta-\theta_0)^2}d\theta}\right]^l\right\} = e^{-r/l_p}\cos(r/R_o)\mathrm{Re}\left\{\left[\frac{\mathrm{erf}[(i+y_1^2(\pi+\theta_0))/\sqrt{2}y_1]-\mathrm{erf}[(i-y_1^2(\pi-\theta_0))/\sqrt{2}y_1]}{\mathrm{erf}\left[(\pi+\theta_0)\frac{y_1}{\sqrt{2}}\right]+\mathrm{erf}\left[(\pi-\theta_0)\frac{y_1}{\sqrt{2}}\right]}\right]^l\right\}, \quad (4)$$

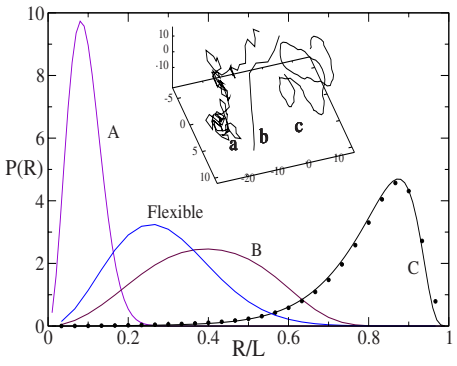


FIG. 2. (Color online) $P(R)$ vs $R/L$ for stiff chains ($L/l_p=1$) for different radii of curvatures, (A) $R_0=0.1$, (B) $R_0=0.3$ and (C) $R_0=10$ (in units of $l_p$). At large $R_0/l_p$ the WLC limit (symbols) is reached while at small $R_0$ the peak of $P(R)$ can go past the flexible limit to smaller values of $R$, and thus can attain a globule size smaller than that of flexible Gaussian chain. We used the same $N$ for all the chains. Inset: typical configurations of (a) flexible, (b) WLC, and (c) intrinsically curved chain. (b) and (c), both have $l_p/L=1$ and (c) in addition has $R_0=0.2$. These configurations were generated using MC simulation.

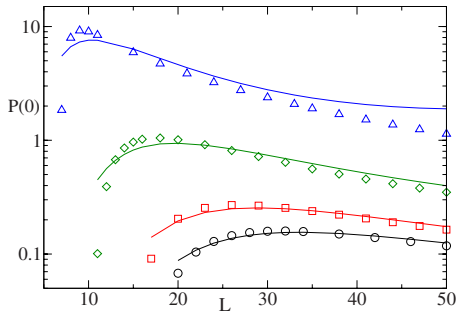


FIG. 3. (Color online) Probability of forming closed loops $P(\mathbf{R}=\mathbf{0})$ versus contour length ($L$), gotten from transfer matrix calculation. From top to bottom $R_0=1.5$, 3, 7.5 and 20, at fixed $l_p=10$. We fitted all the curves (solid lines) with the approximate formula derived by Shimada and Yamakawa [5]: $P(\mathbf{R}=\mathbf{0})=(896.32/l)^5\exp[-14.054/l+0.246l]$, for WLC in the range $l=L/l_p<10$. In these fits $l_p$ was used as an open parameter. For the bottom two curves (small $l_p/R_0$, i.e., WLC limit) the fit is good and $l_p\sim 10$ was reproduced; but for the top two curves (large $l_p/R_0$) the fit fails and yields $l_p\sim 5$. This provides us a diagnostic tool for distinguishing a curved polymer from a WLC. Experimentally, $P(0)$ is measured by counting the fraction of closed loops in an ensemble of mono disperse polymer strands. It is interesting to note that despite an exponentially decaying tangent-tangent correlation function, short curved chains with high $l_p/R_0$ (top two curves) do show a strong tendency to form a flat circular ($R_0$) loop of length $L=2\pi R_0$, even in 3D. The conformation (c) in the inset of Fig. 2 also show such tendency.

where $r=l(L/N)$. For finite $R_0, L$, but large $N$, the $N$-dependent factor $\mathrm{Re}[..]\to 1$ and we get $C(r)=e^{-r/l_p}\cos(r/R_o)$. Thus because of the preferred direction of the angle $\theta_0$ (as opposed to $\pm\theta_0$) the decay is oscillatory. This is analogous to imposing an intrinsic torsion in 3D.

We now compute the distribution function $P(\mathbf{R})$, using transfer matrix methods. We also verified these results using a Monte Carlo (MC) simulation which gave additional insights into the typical configurations of the curved chain (see inset of Fig. 2). The distribution function of the end to end vector $\mathbf{R}$ is $P(\mathbf{R})=C\int d\hat{t}_1\cdots\int d\hat{t}_N e^{-\beta H}\delta(\Sigma_{i=1}^N \hat{t}_i-\mathbf{R})$, where $C$ is the normalization constant for $\int d\mathbf{R}P(\mathbf{R})=1$. Following Ref. [13], $P(\mathbf{R})$ can be connected to the partition function $Z(f)=\int d\hat{t}_1\cdots\int d\hat{t}_N \exp[-\beta H+f\int_{x=0}^{L/Lp}\hat{t}_i^z dx]$, where $f$ is an external field (analogous to external magnetic field in Ising model). This connection is made via the reduced probability distribution $p(z)=\int d\mathbf{R}P(R)\delta(R_3-z)$, which is the probability that one end of the polymer is fixed at $\mathbf{R}=\mathbf{0}$, and the other end lies in a given $z$ plane. Using the definition of $P(\mathbf{R})$ it turns out that the Laplace transform of $p(z)$, $\tilde{p}(f)=\int_{-L}^{L}dz\,\exp(fz/l_p)p(z)=Z(f)/Z(f=0)$. For computation purpose we converted this Laplace transform to a Fourier transform by choosing $f$ purely imaginary. Substituting the Hamiltonian in $Z(f)$ we get $Z(f)=\Sigma_{\hat{t}_1}..\Sigma_{\hat{t}_N}\exp\{\Sigma_{i=1}^{N-1}[h_i+\frac{f\Delta}{2}(\hat{t}_i+\hat{t}_{i+1}).\hat{z}]+\frac{f\Delta}{2}(\hat{t}_1+\hat{t}_N).\hat{z}\}$. $Z(f)$ can be computed using transfer matrices [14].

$$Z(f)=\sum_{\hat{t}_1}\sum_{\hat{t}_N}\langle\hat{t}_1|V^{N-1}|\hat{t}_N\rangle\exp\left\{\frac{f\Delta}{2}(\hat{t}_1+\hat{t}_N)\cdot\hat{z}\right\} \tag{5}$$

where the elements of the transfer matrix $V$ are $\langle\hat{t}_i|V|\hat{t}_{i+1}\rangle=\exp[-h_i+\frac{f\Delta}{2}(\hat{t}_i+\hat{t}_{i+1})\cdot\hat{z}]$. After computing $Z(f)/Z(f=0)$ numerically, we inverse Fourier transform it to obtain $p(z)$ and using the relation $P(R)=-\frac{1}{2\pi z}\frac{dp(z)}{dz}|_{z=R}$ (which is obtained in Ref. [13] using tomographic method and the isotropy of $P(R)$) we obtain $P(R)$.

For semiflexible polymers with intrinsic curvature the energy of a configuration is proportional to $l_p$, at fixed $L$. Therefore at large $l_p$, little deviation of local $R$ from $R_0$ makes the energy cost for such fluctuations large. Such rare but important small angle fluctuations, which requires large sampling in a Monte Carlo simulation, can be efficiently captured by transfer matrix method. In this stiff limit the peak of the end-to-end distribution function $P(R)$ is pushed away from the entropy dominated Gaussian peak (see Fig. 2) and forces the polymer to make circular arcs of radius $R_0$. But at small $R_0$, very small globules, smaller than even that of a flexible Gaussian chain (of same N), can form (Fig. 2). Whereas for small value of $l_p$ the behavior will be dominated by the flexible limit and the peak of $P(R)$ moves toward the Gaussian peak.

In Fig. 3 we show how loop formation probability $P(\mathbf{R}=\mathbf{0})$ changes with contour length, in different regimes of $l_p/R$. Reference [8] had reported similar result using a Monte Carlo sampling. They found that as $R_0$ increases the peak of $P(\mathbf{R}=\mathbf{0})$ unexpectedly shifts to $L$ values lesser than $2\pi R_0$. This was argued as thermal softening of the polymer. But it is unclear why thermal fluctuations should favor larger bending over smaller bending (relative to curvature $R_0^{-1}$). We argue that actually the shift occurs due to the competition between two different peaks in $P(\mathbf{R}=\mathbf{0})$, and it also gives us a diagnostic tool to differentiate a curved chain from a WLC. At small $l_p/R_0$ i.e., in the WLC limit $P(\mathbf{R}=\mathbf{0})$ has a peak at approximately $L/l_p\sim 3$ which emerge from a competition of

bending energy and entropy [5]. Whereas for large $l_p/R_0$ the curved chain has a peak at $L=2\pi R_0$ which is driven by energetics of intrinsic curvature. Notice that for the upper most plot (in Fig. 3) the peak is located at $L/2\pi R_0=1$, while in the lower most plot it is located at $L/l_p\sim 3$. We note that Ref. [8] had fitted their data for $P(\mathbf{R}=\mathbf{0})$ with a formula in Ref. [5], which however was derived for a curved polymer with nonzero torsion.

Our transfer matrix calculation is different from the usual one in that we cannot use periodic boundary condition which allows one to approximate the partition function as $\lambda_{max}^N$, where $\lambda_{max}$ is the largest eigenvalue of the transfer matrix $V$. This is because we work in the regime $l_p\sim L$ where the effect of the boundary conditions can propagate deep inside the chain. In other words, our system size is not larger than the correlation length and hence strong finite size effects are expected. In Eq. (5), $Z(f)$ is obtained as a weighted sum over all the matrix elements of $V^{N-1}$. In order to evaluate $V^{N-1}$ numerically, the angular space $\Omega\equiv(\theta,\phi)$ for a bond vector $\hat{t}_i$ is divided into $n=n_1\times n_2$ bins. Thus the matrix $V$ has dimension $n\times n$. Note that while obtaining $V^{N-1}$ in Eq. (5) a matrix multiplication $V^2=\int d\hat{t}V|\hat{t}\rangle\langle\hat{t}|V$ is numerically implemented through a discrete sum: $[V^2]_{ik}=\int d\Omega_j V(\Omega_i,\Omega_j)V(\Omega_j,\Omega_k)=c\Sigma_{j=1}^n V_{ij}\sin\theta_j\delta_{jl}V_{lk}=c[VSV]_{ik}$. Here the matrix $S_{jl}=\delta_{jl}\sin\theta_j$, with no summation over $j$ intended, [15] arose from $d\Omega_j=\sin\theta_j d\theta_j d\phi_j$ and $c=d\theta d\phi=(\pi/n_1)\times(2\pi/n_2)$. Finally, in order to get $V^{N-1}$ we needed a multiplication of the type $VSVSVS\ldots V$. Since for high $l_p$ and $R_0$, the main contribution to $Z(f)$ comes from configurations where the interbond angles are small (and even smaller if $N$ is increased), the angular discretization has to be dense enough to pick up the contribution from the small interbond angles. This is computationally expensive. So we chose length discretization as $N-2=2^m$ so that using $\Theta(\log_2 N)$ number of matrix multiplications we could obtain the matrix $(VS)^{N-2}$.

Now we discus connection of our model with one of the discrete models for WLC, namely the Freely jointed chain model (FRC) [7]. FRC has fixed bond lengths $b$, with the interbond angles fixed at $\theta_0$. In the continuum limit $\theta_0,b\to 0,N\to\infty$, the quantities $l_p=2b/\theta_0^2$ and $L=Nb$ are finite. So macroscopically there are two scales. Where as in our curved chain model there are three macroscopic scales $L,l_p$ and $R_0$, and thus it is expected to be different from FRC. Only if the dimentionless ratio $l_p/R_0\to 0$ then curved chain model and WLC are identical. We have made this comparison in Figs. 2 and 3.

Is there a limit where our discrete model reduce to FRC? For finite $N$, our model surely has higher entropy than FRC, because both $\phi$ and $\theta$ can vary in our model, where as in FRC $\theta$ is fixed. Here $(\phi,\theta)$ is the orientation of the bond $\hat{t}_{i+1}$ holding the polar axis along $\hat{t}_i$. Quantitatively, in our model the probability of having an interbond angle $\theta$ is $P(\theta)\propto\exp[-h(\theta)]$ [see Eq. (1) and just above Eq. (2)]. In the small $\theta$ limit, expanding $\cos\theta$, we arrive at $h(\theta)=\frac{1}{2\Delta}(\theta-\theta_0)^2$, where $\theta_0=b/R_0$. For large $N$ and finite $L,l_p$, i.e., for $\Delta\to 0,P(\theta)$ is a Gaussian of zero width, equivalently a delta function, reducing our model to FRC. But note that here $\theta_0=\frac{b}{R_0}\sim\Theta(1/N)$, where as in FRC $\theta_0\sim\Theta(1/\sqrt{N})$. So the two models are close only for large $N$, but not identical. It is important to note, that merely the effective persistence length of our model $\tilde{l}_p\to l_p$, for large $N$, does not mean that in the continuum limit the models are identical; difference in the other observables, namely, $P(R)$ and loop formation probability $P(0)$ do indicate that there exists another important macroscopic length scale $R_0$.

In summary, we showed by exact calculation that both in 2D and 3D, intrinsically curved polymers give exponentially decaying tangent correlation, $C(r)$, as semiflexible polymers. But the apparent persistence length $\tilde{l}_p$ is substantially lesser than $l_p$ for short chains, when the ratio $l_p/R_0$ is large. Contrary to physical expectation $C(r)$ does not have oscillatory decay with period $L=2\pi R_0$, unless we impose torsion in 3D or fix the sign of the preferred interbond bending angle in 2D. Curved biofilaments of FtsZ or tubulin can be distinguished from WLCs' through loop formation probabilities, which has not been measured yet for curved polymers.

We thank the Department of Science and Technology, India for financial support.

[1] M. Caplow, R. L. Ruhlen, and J. Shanks, J. Cell Biol. **127**, 779 (1994); M. I. Molodtsov *et al.*, Proc. Natl. Acad. Sci. U.S.A. **102**, 4353 (2005).
[2] D. Popp *et al.*, Biopolymers **91**, 340 (2009).
[3] J. Mingorance *et al.*, J. Biol. Chem. **280**, 20909 (2005).
[4] B. Ghosh and A. Sain, Phys. Rev. Lett. **101**, 178101 (2008).
[5] H. Yamakawa, Macromolecules **10**, 692 (1977); J. Shimada and H. Yamakawa, *ibid.* **17**, 689 (1984).
[6] J. Moukhtar *et al.*, Phys. Rev. Lett. **98**, 178101 (2007).
[7] M. Doi and S. F. Edwards, *The Theory of Polymer Dynamics* (Clarendon Press, Oxford University Press, Oxford, 1986).
[8] S. Rappaport and Y. Rabin, Macromolecules **37**, 7847 (2004).
[9] A. Craig and E. M. Terentjev, Macromolecules **39**, 4557 (2006).
[10] R. E. Goldstein and S. A. Langer, Phys. Rev. Lett. **75**, 1094 (1995).
[11] M. E. Fisher, Am. J. Phys. **32**, 343 (1964); L. D. Landau, *Statistical Physics* (Pergamon Press, Oxford, 2002).
[12] C. Yuan, H. Chen, X. W. Lou, and L. A. Archer, Phys. Rev. Lett. **100**, 018102 (2008).
[13] J. Samuel and S. Sinha, Phys. Rev. E **66**, 050801(R) (2002).
[14] P. Ranjith, P. B. Sunil Kumar, and G. I. Menon, Phys. Rev. Lett. **94**, 138102 (2005).
[15] D. Bensimon, D. Dohmi, and M. Mezard, Europhys. Lett. **42**, 97 (1998).